Volume 14 | Number 21 | 7 November 2014 | Pages 4107–4296

Lab on a Chip

Miniaturisation for chemistry, physics, biology, materials science and bioengineering

www.rsc.org/loc

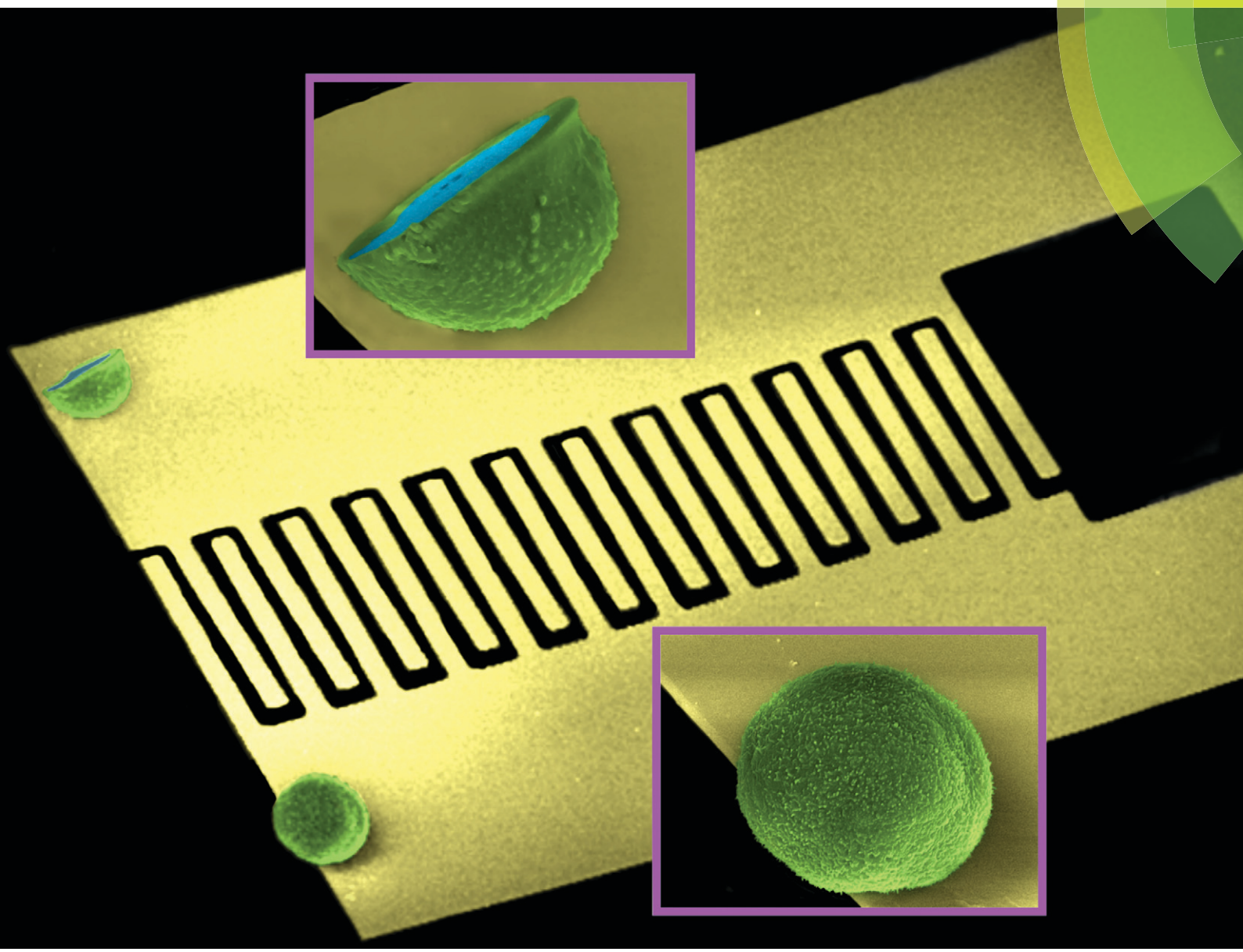

ISSN 1473-0197

ROYAL SOCIETY OF CHEMISTRY

PAPER

Cagri A. Savran *et al.*

On-demand weighing of single dry biological particles over a 5-order-of-magnitude dynamic range

Lab on a Chip

PAPER

View Article Online
View Journal | View Issue

Cite this: *Lab Chip*, 2014, **14**, 4188

On-demand weighing of single dry biological particles over a 5-order-of-magnitude dynamic range

Bin-Da Chan,[ac] Kutay Icoz,[bcd] Wanfeng Huang,[ac] Chun-Li Chang[ac] and Cagri A. Savran*[acd]

Received 1st July 2014,
Accepted 5th August 2014

DOI: 10.1039/c4lc00765d

www.rsc.org/loc

We report a simple and highly versatile system to select and weigh individual dry biological particles. The system is composed of a microtweezer to pick and place individual particles and a cantilever-based resonator to weigh them. The system can weigh entities that vary from a red blood cell (~10^{-11} g) to the eye–brain complex of an insect (~10^{-6} g), covering a 5-order-of-magnitude mass range. Due to its versatility and ease of use, this weighing method is highly compatible with established laboratory practices. The system can provide complementary mass information for a wide variety of individual particles imaged using scanning electron microscopy and determine comparative weights of individual biological entities that are attached to microparticles as well as weigh fractions of individual biological entities that have been subjected to focused ion beam milling.

Introduction

Measuring the dry mass of entities has sparked great interest because this simple physical property can provide unique insight into many fields including biology, pathology, and ecology. For example, studies showed that the dry mass of individual yeasts could be used as an effective tool to study the synthesis of new cellular material during cell growth.[1,2] Researchers also used the dry mass to monitor the growth of cells[3,4] as well as to demonstrate the change in cell mass in response to chemicals.[5,6] In several studies of environmental biology and ecology, it was demonstrated that the mass of airborne pollens can be correlated with the pollen transportation and gene flow.[7–9] The dry mass of microorganisms was also used to determine the metabolic rate that represented the energy needed to sustain life.[10–12]

Several approaches regarding the measurement of the dry mass of biological microparticles have been reported. It has been shown that the dry mass of bacteria can be estimated by using their carbon content[13] or electron opacity values determined by electron microscopy.[14] Optical interferometry methods[4,15–19] were also used to observe temporal changes in the dry mass of live cells. However, to use methods that do not directly weigh particles, assumptions about their optical or material properties have to be made. In addition, the accuracy of measurement can be affected by experimental conditions such as debris in fluid[18] or speckles generated by the illumination sources.[4] Researchers have used nanomechanical resonance to demonstrate characterization of cells in terms of their mass.[18,20–22] For example, Manalis' group used suspended microchannel resonators (SMRs) to estimate the dry mass of cells in suspensions that flow through the interior channels of a microfluidic structure.[23,24] Here, we report a systematic approach to directly measure the dry mass of individually selected biological microparticles over a 5-order-of-magnitude dynamic range from 30 pg to 2.4 μg.

Cells and microorganisms are often dried to obtain their scanning electron microscopic (SEM) images. With proper fixation and drying procedures,[25] the geometries and interior structures of dried samples can be preserved and recognized under an electron microscope. Several studies have reported using the electron microscope to conduct pathological or morphological analyses of dried biological microparticles including cancer cells,[26] *Drosophila* embryos,[27,28] erythrocytes,[29,30] and pancreatic islets.[31–34] In addition to SEM imaging, drying procedures are also used in conjunction with other procedures and tests such as focused ion beam milling,[35] microorganism preservation,[36] and mass spectrometry.[37] With the method we present here, the mass of a wide variety of dried biological particles can be directly and individually measured and can be readily used to complement their morphological, structural or chemical properties.

[a] *School of Mechanical Engineering, Purdue University, West Lafayette, IN, 47907, USA. E-mail: savran@purdue.edu*
[b] *Electrical and Electronics Engineering, Abdullah Gül University, Kayseri, 38039, Turkey*
[c] *Birck Nanotechnology Center, Purdue University, West Lafayette, IN, 47907, USA*
[d] *Weldon School of Biomedical Engineering, West Lafayette, IN, 47907, USA*

The weighing system comprises a micromanipulator and a cantilever-based resonator. Under a microscope, a chosen microentity can readily be picked up by the micromanipulator and placed onto an arm of the resonator for weighing (Fig. 1a).[38] Once the target microparticle is located on the tip of the cantilever, the resulting change in the resonance frequency of the loaded cantilever is observed. This change in the resonance frequency reveals the mass of the loaded entity.[39] The advantage of this system is its ability to pick-and-weigh an individually selected particle as opposed to relying on the random adsorption of a number of particles onto a sensor surface. This report presents the weighing of a wide variety of microparticles ranging from single cells to the eye–brain complex of larval *Drosophila*.

Materials and methods

A. Measurement principle

In a previous study, we demonstrated that the micromanipulator, which is composed of an elastically deformable silicon tweezer structure and a micrometer head for manual actuation, was able to grab microparticles and position or arrange them into patterns and structures.[38] We also demonstrated preliminary experiments by placing individual particles on resonating cantilever surfaces for weighing.[39] The dual cantilever design of our microresonator enables two simultaneous weight measurements. Oftentimes, one of the cantilevers serves as a reference to test the operation of the system (before an experiment) by using a load of known mass. The reference cantilever can also serve to account for small disturbances that may affect both cantilevers.[39] A piezoelectric actuator (Thorlabs AE0203D04F) is used to drive the resonators. A laser beam (Newport R-30091, 5 mW) is used to illuminate the interdigitated fingers between the two cantilevers to generate a reflective diffraction pattern. The resonance frequency of each cantilever is obtained in a single measurement by observing the intensity of the 0^{th}-order reflected diffraction mode that changes in accordance with the deflection between the two cantilevers.[40]

The cantilevers are 250 μm in length, 500 nm in thickness, and 50 and 60 μm in width at the base and the tip, respectively. The interdigitated fingers are 50 μm in length and 5 μm in width with a 3 μm spacing between each finger (Fig. 1a). Each cantilever is constructed by a 480 nm thick silicon-rich silicon nitride layer deposited with a 20 nm thick gold thin film. We estimate the effective density of the cantilever to be 3.65 g cm^{-3} by considering the thicknesses and

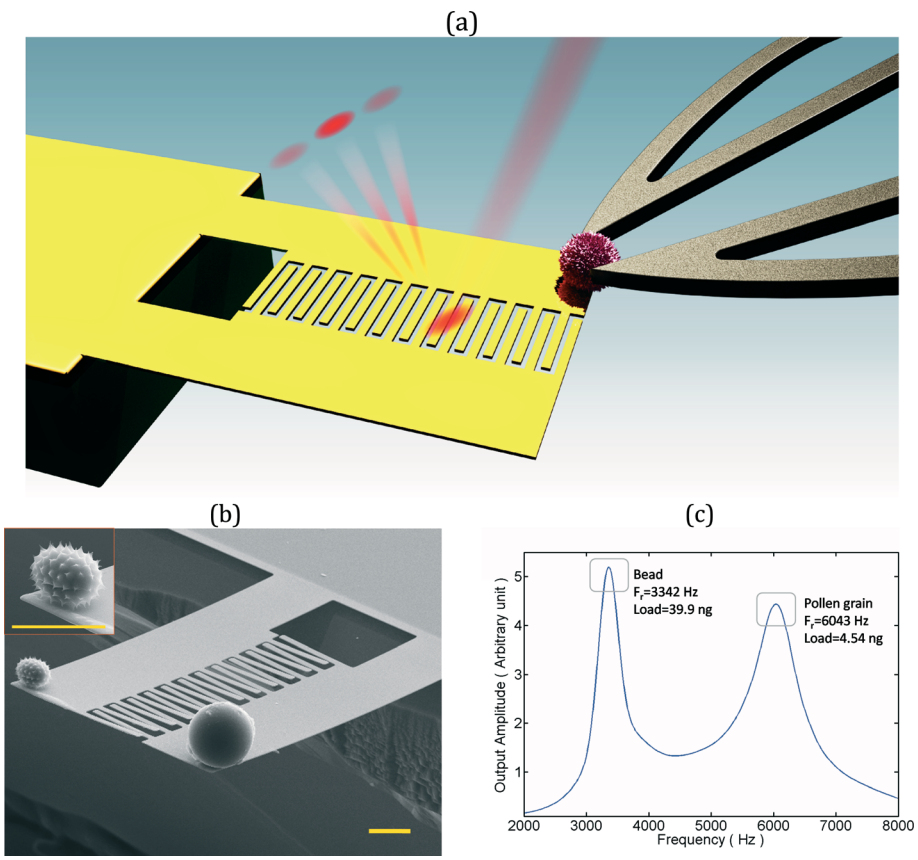

Fig. 1 (a) Schematic of the weighing system. The target microparticle is grabbed by a micromanipulator and placed onto the tip of a cantilever-based resonator for weighing. The added mass is derived by observing the resonance frequency of the loaded cantilever. (b) SEM image of a pollen grain placed on a cantilever (left arm). The reference cantilever (right arm) was loaded with a polystyrene bead of known mass. Scale bars: 30 μm. (c) Frequency response of the system that shows the resonance frequencies of both cantilevers.

densities of gold (19.3 g cm^{-3})[41] and silicon nitride (3 g cm^{-3}).[42] The Young's modulus of the cantilever is determined to be 170 GPa by matching the measured resonance frequency with that obtained by finite element simulation.

It is known that the resonance frequency of a cantilever depends not only on the mass of the load but also on the location of the load with respect to the tip of the cantilever.[39,43] Therefore, in each experiment, the exact location of a loaded particle is determined by optical microscopy. Afterward, the resonance frequency of a loaded cantilever and the location of the added mass are used in an ABAQUS finite element simulation to determine the added mass. Fig. 1b demonstrates the weighing of a *Lasthenia fremontii* pollen grain (left arm). Prior to the placement of an entity, a small amount of grease (around 100 to 300 pg) is often smeared on the cantilevers to improve the adhesion between the loaded particle and the cantilever surface. The frequency shift resulting from the grease is taken into account by measuring the resonance frequency of the cantilever with the grease on it. On the right arm, a polystyrene bead with a previously measured mass of 39.9 ng is loaded to ensure that the system is functioning properly. Fig. 1c is the experimental frequency spectrum corresponding to the weighing experiment in Fig. 1b. The resonance frequency of the sensor cantilever shifted from 7319 Hz (the resonance frequency of an empty cantilever) to 6043 Hz due to the loading of the pollen grain. The resonance frequency of the reference cantilever was reduced to 3342 Hz due to the weight of the reference bead. By matching these experimentally determined frequencies and the microscopically verified locations of the particles with the results of our finite element simulation, the mass of the pollen grain in Fig. 1c was obtained as 4.54 ng.

B. Cultivation of cancer cell lines

Human cancer cell lines were cultured, fixed and dried for weighing experiments. The breast cancer cell line MCF-7, obtained from American Type Culture Collection (ATCC), was cultured in Eagle's Minimum Essential Medium (EMEM, ATCC) with 10% fetal bovine serum (FBS, Gemini Bio Products). The lung cancer cell line A549, obtained from Indiana University School of Medicine, was cultured in F-12K Medium (ATCC) with 10% FBS. KB cells, a HeLa subclone obtained from Purdue University Department of Chemistry, were cultured in folic acid-depleted RPMI 1640 medium (Gibco) with 10% FBS. All three cell lines were harvested using trypsin-EDTA (Invitrogen) before going through a series of fixing, dehydration, and drying processes, which are further described in the section "Fixation, dehydration and drying of cell samples".

C. Preparation of blood cells

Red blood cells (RBCs) and leukocytes were isolated from blood samples of healthy donors under an approved IRB protocol and subjected to weight measurement. Blood samples were first collected in BD Vacutainer tubes to which was added sodium polyanethol sulfonate (SPS) and kept at 4 °C immediately after collection until blood cell isolation. Blood samples were used within 2 hours after collection. To obtain RBCs, 4 mL of the collected blood was first transferred into a tube and centrifuged at 400*g* for 20 minutes. RBCs were subsequently collected from the bottom of the tube using a pipet tip. Leukocytes (mainly lymphocytes) were isolated from another 4 mL of blood using Ficoll-Paque PLUS (GE Healthcare) by following the standard protocols provided by the vendor.

D. Preparation of other biological microparticles

Pollen grains from *Lasthenia fremontii* and *Lasthenia glabrata* species were obtained from Purdue University Department of Biological Sciences. Pollen grains were collected on glass slides by tapping the flowers that contained the grains. Afterward, individual pollen grains were directly grabbed by the micromanipulator for weighing. Mouse prostate stem cell spheres were provided by Purdue University Center for Cancer Research. Stem cell spheres were fixed with paraformaldehyde after isolation from Matrigel (BD Bioscience). Mouse pancreatic islet spheroids were provided by the Department of Agricultural and Biological Engineering, Purdue University. The eye–brain complexes of larval *Drosophilae* were provided by the Department of Biochemistry, Purdue University.

E. Fixation, dehydration and drying of cell samples

Cells and microorganisms were first fixed with 2% glutaraldehyde in 0.1 M cacodylate for 30 minutes. After rinsing with the cacodylate buffer (0.1 M, pH 7.4), cells and microorganisms were post-fixed with 1% osmium tetroxide (OsO_4) in 0.1 M cacodylate for 30 minutes. These two fixation steps can effectively retain proteins and lipids in cells[44,45] and have been commonly used as methods to stabilize the interior structures of cells and tissues when preparing them for SEM and dissection.[46,47] The samples were then subjected to a series of dehydration processes in ethanol with varying concentrations (10, 30, 50, 70, 90, and 100% for 10 minutes each). Afterward, the cells were resuspended in 50% and 100% hexamethyldisilazane (HMDS) solutions for 10 minutes each. The use of HMDS has been shown as an economical and effective alternative to the critical point drying (CPD) method for drying of biological samples.[48–50] It has been demonstrated that HMDS induces only a small amount of surface tension and hence prevents cell structures from collapse and distortion that may be introduced during air-drying.[51–53]

Results and discussion

A. System calibration and uncertainty analysis

We first verified the accuracy of our weighing scheme by comparing the effective density of polystyrene beads, determined by measuring their mass and microscopically observing their volume, to their density reported by the

manufacturer (Spherotech, Inc.). In this test, we individually characterized the mass and volume of ten small (measured average diameter: 24.8 μm) and ten large (measured average diameter: 41.9 μm) polystyrene beads. The measured average masses of the small and large beads were 8.37 and 40.62 ng, respectively. The average densities of ten different beads were then calculated as 1.048 g cm^{-3} for the small beads and 1.055 g cm^{-3} for the large beads. These results were in good agreement with the density of polystyrene beads reported by the manufacturer (~1.05 g cm^{-3}).

To evaluate the systematic uncertainty in our mass measurements, we investigated the uncertainty in determining the location of a loaded particle as well as that in our frequency measurements. The uncertainty in the loading location is introduced by the resolution limit of the optical microscope used. The uncertainty in the frequency measurement is due to the effects of both the quality factor of the cantilever and the signal-to-noise ratio of the measurement.[39] To quantify the uncertainty in both the location and the frequency measurements, we conducted experiments in which we repeatedly measured the resonance frequency of a cantilever and the location of a polystyrene particle loaded on a cantilever. The location of the polystyrene bead (24.8 μm in diameter) was repeatedly measured (20 times) by means of a calibrated bright-field microscope. The location of the bead was, on average, 8.3 μm away from the tip of the cantilever, and the 99.7% confidence interval for the resulting uncertainty in this location was determined to be ±0.16 μm. The uncertainty in the resonance frequency was obtained by measuring the resonance frequency of the loaded cantilever ten times. The average resonance frequency was measured to be 3345 Hz (which gave the mass of the bead as 39.7 ng) with an uncertainty of ±0.89 Hz at the 99.7% confidence level.

The effect of the uncertainties in the measured location (δx) and frequency (δf) on the uncertainty in the mass measurement (δm) was then calculated using an error propagation approach:

$$\delta m = \sqrt{\left(\frac{\partial m}{\partial f}\delta f\right)^2 + \left(\frac{\partial m}{\partial x}\delta x\right)^2}. \quad (1)$$

Here, m is the mass of the load (kg), x is the distance of the weighed particle from the tip of the cantilever (m), and f is the natural frequency of the cantilever (Hz) given by:[43,54]

$$f = \frac{1}{2\pi}\sqrt{\frac{K}{M + \left[1 - \frac{3}{2}\left(\frac{x}{L}\right) + \frac{1}{2}\left(\frac{x}{L}\right)^3\right]^2 m}} \quad (2)$$

where L is the length of the cantilever (m), M is the effective modal mass of the cantilever (kg), and K is the stiffness of the cantilever (N/m). The stiffness of our cantilever (K) was determined to be 0.0182 N/m by simulating the tip deflection due to a point load using finite element simulation. Next, the effective mass (M) was determined to be 8.6 ng by using K and the measured natural frequency of an empty cantilever. Fig. 2a shows the dependence of the calculated mass uncertainty (δm) on the added mass (m) and on the loading location (x). According to Fig. 2a, the uncertainty in mass is 3.2 pg for a 1 ng load (when x = 0). This uncertainty increases to about 82 pg when the added mass is 40 ng. The effect of the location is less severe as the uncertainty in the mass of a 1 ng load increases only from 3.2 pg to 3.8 pg when x increases from 0 to 20 μm.

We next compared the calculated uncertainties with the experimentally observed variations in mass. We used two groups of 10 beads for this analysis, one group with an average diameter of 24.8 μm ("small beads") and one with an average diameter of 41.9 μm ("large beads"). We first picked one bead from each group and weighed it 10 times. Each weighing was performed from scratch where the same bead was weighed, removed from the cantilever surface, placed back on the cantilever and weighed again by recording the new frequency and bead location. The resulting variation in mass measurements as well as the systematic uncertainty predicted by (1) at the 99.7% confidence level is shown in Fig. 2b. The similarity between the experimental and the

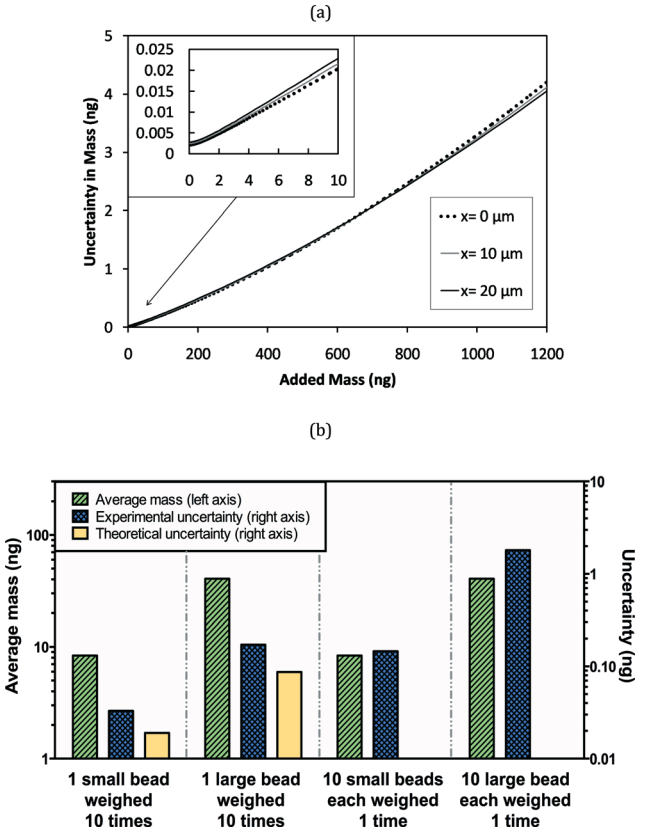

Fig. 2 (a) The theoretical uncertainty in measured mass with respect to the mass and the distance of the loaded particle with respect to the cantilever tip. (b) The bar chart illustrates experimental and theoretical uncertainties in mass for single beads (n = 10). The average masses and experimental uncertainties in mass of ten different beads are also presented.

calculated uncertainty values indicates that the uncertainties in the frequency and location measurements are an important part of the overall systematic uncertainty. Next, we studied the variation of mass from one bead to another in each group wherein we weighed each bead from each group once. These results are also presented in Fig. 2b and in Table 1. The results show that the bead-to-bead variation in mass, even for beads from the same group, greatly outweighs the systematic uncertainty in the mass measurements.

B. Arrangement of single particles on the resonator surface

In an earlier study, we demonstrated the capability of particle-by-particle construction of microstructures on various substrates including surfaces of sensors fabricated by standard microelectronic fabrication processes.[38] With this capability, we can build structures by combining individual particles on the tip of a resonator and readily weigh these structures. This becomes especially useful for weighing particles smaller than ~15 μm. It is often easier to maneuver and place a small particle on top of a larger spherical particle already placed on the cantilever surface than it is to directly place it on the two-dimensional cantilever surface. Fig. 3a shows an example of a cell–bead stack built on a cantilever surface. To build this stack, a polystyrene bead (orange) was first placed on the cantilever. Next, the top of the bead was "painted" with a layer of grease (purple) to improve adhesion. Afterward, an individually targeted KB cell (green) was placed on the bead using the micromanipulator.

To obtain the mass of the specific KB cell in Fig. 3a, the resonance frequency of the cantilever with the bead/grease combination was first determined. After the cell was placed on top of the bead, the resonance frequency of the cantilever corresponding with the bead/grease/cell combination was measured again. Subsequently, the measured resonance frequencies as well as the locations of the bead and cell were used in finite element simulation to determine the mass of the cell. The mass of the dry KB cell in Fig. 3a was determined to be 0.52 ± 0.019 ng (measured mass ± theoretical systematic uncertainty). We also applied the method to weigh smaller biological particles such as red blood cells (Fig. 3b). The resulting mass of the specific dry red blood cell in Fig. 3b was 57 ± 18 pg. Note that in this case, using a heavier base particle under the relatively small red blood cell increases the systematic uncertainty. Therefore, the measurement resolution can be improved by choosing a lighter base particle such as a smaller bead.

C. Weighing of individually selected cancer cells

Knowing the mass of a cell can be extremely valuable. For example, researchers have shown that they can investigate the effects of chemicals on tumor cells by observing their masses.[5,55] It has also been shown that the mass of cells can be associated with cellular senescence and cell growth.[56,57] With our approach, a particular cell can be individually isolated and weighed. Fig. 4a shows individual cancer cells that were selectively weighed. In this experiment, five A549 cancer cells were selected from the surface of a glass slide that contained numerous dried A549 cells and weighed. After weighing, the A549 cells were removed from the cantilever surface and arranged on a conductive substrate for SEM

Table 1 Experimental and theoretical mass uncertainties at the 99.7% confidence level

Sample	Mean mass (ng)	Experimental error (±ng)	Theoretical error (±ng)
1 small bead weighed 10 times	8.38	0.033	0.019
1 large bead weighed 10 times	40.56	0.172	0.087
10 small beads each weighed 1 time	8.37	0.146	NA
10 large beads each weighed 1 time	40.62	1.810	NA

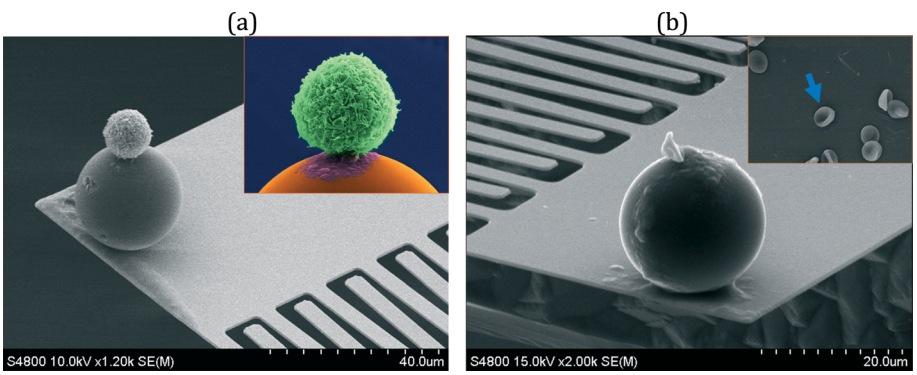

Fig. 3 SEM images of microparticles weighed by the cantilever-based resonator. (a) A KB cell was placed on top of a polystyrene bead for weighing. The inset shows the side view of the artificially colored cell–bead stack. Green indicates the KB cell, purple the adhesive grease layer, and orange the polystyrene bead. (b) Weighing of a red blood cell. A red blood cell was individually picked up from a group of cells (inset) by the micromanipulator.

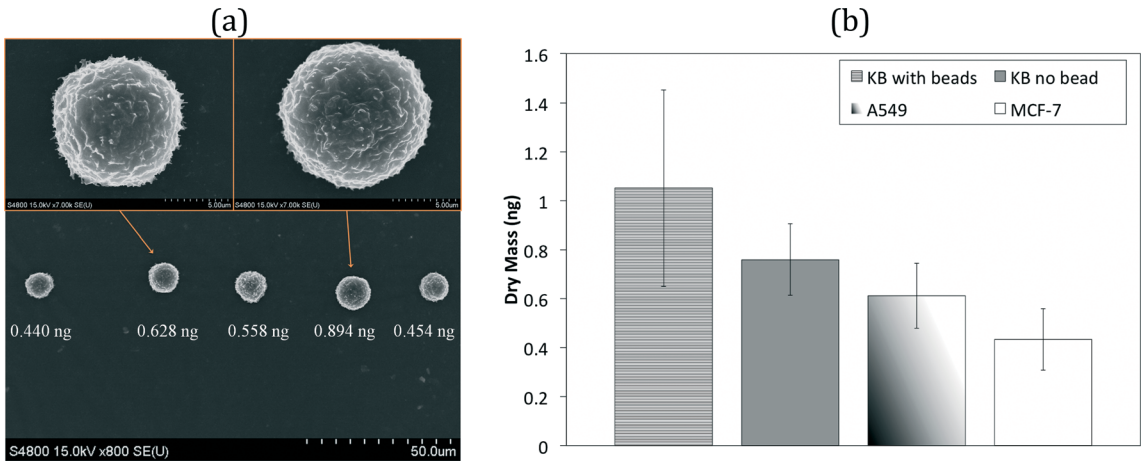

Fig. 4 (a) SEM images of weighed A549 cells with their corresponding dry masses. The theoretical uncertainty in the mass measurement was around 20 pg. (b) The dry masses of bead-bound KB cells, bare KB cells, and A549 and MCF-7 cancer cells. Error bars represent the ±99.7% confidence interval of cell-to-cell variation.

imaging. With this particular protocol that combines SEM imaging and *on-demand* weighing, detailed spatial information as well as the mass of individual cells can be obtained, as shown in Fig. 4a.

The developed method can also be used to characterize individual cells that are attached to other particles. For example, magnetic particles are frequently used in immunomagnetic separation to isolate specific cells from heterogeneous suspensions.[58,59] This analysis often relies on the balance among magnetic, fluidic and gravitational forces applied on cells and hence the mass of the individual cell–bead assembly. Using our method, the mass of an individual cell that is attached to magnetic particles can be determined and compared to that without particles. This information can be useful for accurate simulations of magnetic flow-based separation systems and the overall optimization of the system.[60,61] Here, we incubated KB cells with magnetic beads (Sigma-Aldrich) conjugated with antibodies against folate receptor (anti-FR, R&D Systems) for 90 minutes. Afterward, bead-bound cells were collected by a magnet[62] and resuspended in a fixing agent (glutaraldehyde). After a series of fixation, dehydration and HMDS-drying steps described before, individual bead-attached and bare KB cells were analyzed using our weighing system.

Fig. 4b shows a comparison of groups of individually weighed KB (with and without beads) and A549 cells as well as MCF-7 cancer cells. The average dry masses of bead-bound KB, bare KB, A549, and MCF-7 cells were measured as 1.05 ± 0.40 ng, 0.76 ± 0.15 ng, 0.61 ± 0.13 ng, 0.43 ± 0.13 ng, respectively (mean ± 99.7% confidence interval, Fig. 4b). The error bars in Fig. 4b indicate the cell-to-cell variation in mass not the systematic measurement uncertainty, which is less than 20 pg. It was observed that dried KB cells were, on average, the heaviest of all three cell lines, whereas MCF-7 cells were the lightest. For KB cells, it was observed that bead-bound KB cells were, on average, 0.29 ng heavier than bare KB cells. The greater variation observed in the mass of bead-bound KB cells is expected and most likely due to variation in the number of beads bound to each cell during incubation.

The method can also be utilized to individually characterize fragments or parts of whole cells. To demonstrate this capability, an individual KB cell was chosen from an array of KB cells that have been weighed individually (Fig. 5a). The targeted cell was sectioned by means of focused ion beam (FIB) milling, as illustrated in Fig. 5b–d. After the milling process, the remainder of the target KB cell was picked up by

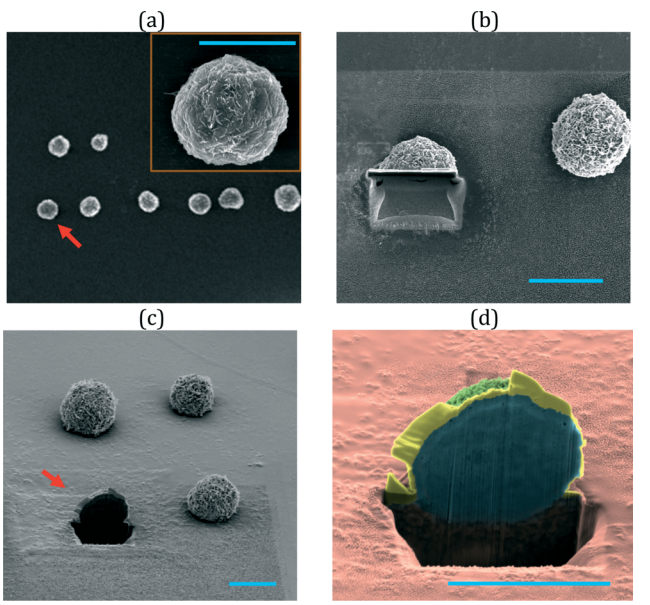

Fig. 5 (a) SEM image of an array of KB cells arranged individually after weighing. The red arrow indicates the specific cell to be milled by FIB. (b) Top view and (c) tilted view of the milled cell. (d) SEM image illustrates the artificially colored cross-section of the milled KB cell. The green and blue parts represent the surface and the interior of the cell, respectively, the yellow part is the thin platinum layer that is deposited to protect and define the milling edge, and the pink part depicts the conductive substrate. Scale bars: 10 μm.

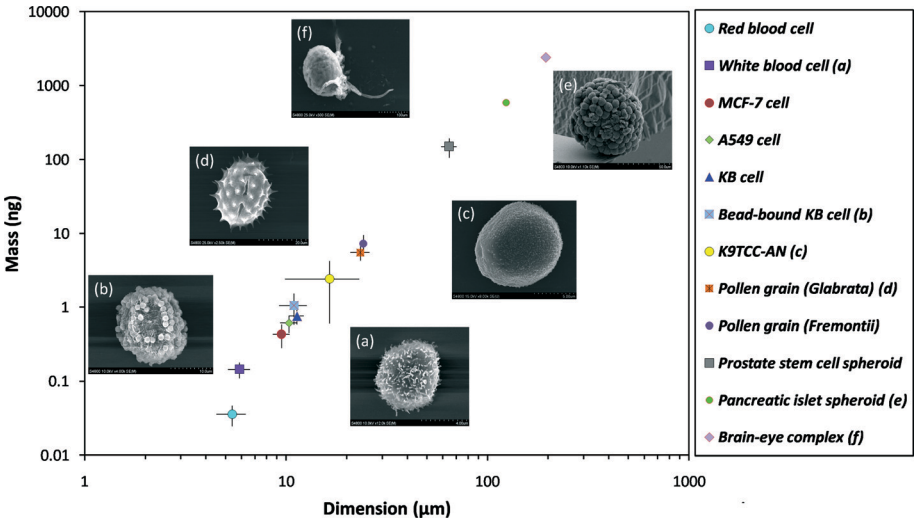

Fig. 6 Measured mass *vs.* dimension of biological microparticles. Insets show the SEM images of the analyzed particles including (a) a white blood cell, (b) a bead-bound KB cell, (c) a K9TCC-AN cell, (d) a *Lasthenia glabrata* pollen grain, (e) a pancreatic islet spheroid from a mouse, and (f) an eye–brain complex collected from a larval *Drosophila*. Error bars represent the ±99.7% confidence interval of sample-to-sample variation when multiple samples were available. Pancreatic islet spheroid and eye–brain complex have a sample size of 1; therefore, no error bars are shown.

Table 2 Measured mass and dimensions of biological microentities. Dimension indicates the diameter of a spherical particle or the largest dimension of a non-spherical particle such as a pollen grain. Mass and dimension variations represent the 99.7% confidence interval of sample-to-sample variation

Sample	Sample size	Average mass (ng)	Mass variation (±ng)	Average dimension (μm)	Dimension variation (±μm)
Red blood cell	10	0.04	0.01	5.41	0.90
White blood cell	9	0.14	0.03	5.88	0.74
MCF-7 cell	20	0.43	0.15	9.51	0.91
A549 cell	20	0.61	0.16	10.36	1.01
KB cell	20	0.76	0.17	11.33	0.94
Bead-bound KB cell	20	1.05	0.47	10.97	1.72
K9TCC-AN	9	2.41	1.8	16.48	6.6
Pollen grain (*Glabrata*)	14	5.51	1.24	23.42	2.56
Pollen grain (*Fremontii*)	14	7.28	2.25	24.25	1.01
Stem cell spheroid	10	149.56	44.24	64.63	5.79
Islet spheroid	1	586	NA	124	NA
Eye–brain complex	1	2395	NA	195	NA

the micromanipulator and weighed again. It was observed that the dry mass of the specific cell in Fig. 5 was reduced from 790 ± 19 pg (measured mass ± theoretical systematic uncertainty) to 220 ± 19 pg after the milling process. FIB milling is generally used to prepare sections of samples for electron microscopy analysis while avoiding the distortion in cellular structures that can result from conventional mechanical sectioning processes.[63] Our system can readily be combined with FIB milling to investigate parts of individual cells or various biological particles in terms of their mass.

D. Characterization of biological microparticles over a high dynamic range

The main advantage of the weighing scheme is its robustness and versatility in selectively weighing individual microparticles over a 5-order-of-magnitude dynamic range of mass. The specific prong design allows the manipulation of particles with dimensions between 5 μm and 300 μm.[38] The large surface area (50 μm by 250 μm) of the cantilever accommodates microparticles with various dimensions. We measured the dry mass of a wide variety of microparticles including (in the order of increasing size) red blood cells, white blood cells, cancer cells, canine transitional cell carcinoma (K9TCC-AN) cells, pollen grains, stem cell spheroids, pollen grains, and pancreatic islet spheroids as well as the eye–brain complexes of insects. Fig. 6 and Table 2 summarize the results of a combined weighing and SEM analysis performed on 12 different kinds of entities. The dimensions of the measured particles ranged from 5.4 μm (red blood cells) to 190 μm (eye–brain complex of larval *Drosophila*). Here, the error bars represent the sample-to-sample variation for all data points except the pancreatic islet and the brain–eye complex where only one sample was available for analysis. For these two data points, the systematic measurement uncertainties are 1.66 ng and 10.25 ng, which are too small to visualize in Fig. 6.

Conclusion

We developed a system capable of individually picking and weighing a wide variety of dry biological particles. The system is based on the combination of a mechanically actuated micromanipulator and a nanomechanical resonator and was designed to mimic the simple and intuitive nature of a typical select-and-weigh experience in a supermarket. We weighed a wide variety of individual biological microparticles whose masses ranged from 10s of picograms to micrograms. The weighed specimens included various cells that are bound by secondary inorganic microparticles, individual pollen grains, and spheroids as well as organs of insects. When used in conjunction with focused ion beam milling, the system can also be used to weigh parts of whole cells. We expect this versatile system to have a wide range of applications including analysis of individual cell's response to drugs or chemical treatments and comparative analysis of individual pollen grains as well as offering interesting possibilities such as autopsy of insects.

Acknowledgements

The authors thank Dr. Shadia Jalal from Indiana University School of Medicine for providing the A549 cell line, Dr. Philip Low from Purdue University Department of Chemistry for providing the KB cell line, Dr. Nancy C. Emery from Purdue University Department of Biological Sciences for providing the pollen grains, Dr. Timothy Ratliff and Hsing-Hui Wang from Purdue University Center for Cancer Research for providing the mouse prostate stem cell spheres, Dr. Vikki M. Weake and Jingqun Ma from Purdue University Department of Biochemistry for providing the eye–brain complexes of larval *Drosophilae*, Dr. Jenna Rickus from Purdue University Agricultural and Biological Engineering for providing the mouse pancreatic islet spheroids, Dr. Deepika Dhawan from Purdue University Department of Veterinary Clinical Sciences for providing the K9TCC-AN cells, and Laurie M. Mueller from Purdue University Life Science Microscopy Facility for coaching the cell fixation and HMDS-drying procedures as well as conducting the cell milling process. This work was supported by a National Science Foundation Award 1343069.

References

1 J. M. Mitchison, *Theor. Biol. Med. Modell.*, 2005, **2**, 4.
2 J. M. Mitchison, *Exp. Cell Res.*, 1957, **13**, 244–262.
3 G. Popescu, Y. Park, N. Lue, C. Best-Popescu, L. Deflores, R. R. Dasari, M. S. Feld and K. Badizadegan, *Am. J. Physiol.*, 2008, **295**, C538–C544.
4 M. Mir, Z. Wang, Z. Shen, M. Bednarz, R. Bashir, I. Golding, S. G. Prasanth and G. Popescu, *Proc. Natl. Acad. Sci. U. S. A.*, 2011, **108**, 13124–13129.
5 L. Weiss, *Exp. Cell Res.*, 1958, **14**, 80–83.
6 W. H. Grover, A. K. Bryan, M. Diez-Silva, S. Suresh, J. M. Higgins and S. R. Manalis, *Proc. Natl. Acad. Sci. U. S. A.*, 2011, **108**, 10992–10996.
7 L. M. Sosnoskie, T. M. Webster, D. Dales, G. C. Rains, T. L. Grey and A. S. Culpepper, *Weed Sci.*, 2009, **57**, 404–409.
8 D. E. Aylor, *J. Aerosol Sci.*, 2002, **33**, 1601–1607.
9 R. van Hout and J. Katz, *J. Aerosol Sci.*, 2004, **35**, 1369–1384.
10 E. A. Dawes and D. W. Ribbons, *Annu. Rev. Microbiol.*, 1962, **16**, 241–264.
11 A. M. Makarieva, V. G. Gorshkov, B. L. Li, S. L. Chown, P. B. Reich and V. M. Gavrilov, *Proc. Natl. Acad. Sci. U. S. A.*, 2008, **105**, 16994–16999.
12 A. Jakubowska and R. Korona, *PLoS One*, 2012, **7**, e33132.
13 G. Bratbak, *Appl. Environ. Microbiol.*, 1985, **49**, 1488–1493.
14 M. Loferer-Krossbacher, J. Klima and R. Psenner, *Appl. Environ. Microbiol.*, 1998, **64**, 688–694.
15 R. Barer, *Nature*, 1952, **169**, 366–367.
16 H. G. Davies and M. H. Wilkins, *Nature*, 1952, **169**, 541.
17 R. Barer, *Nature*, 1953, **172**, 1097–1098.
18 G. Popescu, K. Park, M. Mir and R. Bashir, *Lab Chip*, 2014, **14**, 646–652.
19 K. Lee, K. Kim, J. Jung, J. Heo, S. Cho, S. Lee, G. Chang, Y. Jo, H. Park and Y. Park, *Sensors*, 2013, **13**, 4170–4191.
20 E. A. Corbin, B. R. Dorvel, L. J. Millet, W. P. King and R. Bashir, *Lab Chip*, 2014, 1401–1404.
21 Y. Weng, F. F. Delgado, S. Son, T. P. Burg, S. C. Wasserman and S. R. Manalis, *Lab Chip*, 2011, **11**, 4174–4180.
22 A. K. Bryan, V. C. Hecht, W. Shen, K. Payer, W. H. Grover and S. R. Manalis, *Lab Chip*, 2014, **14**, 569–576.
23 F. Feijo Delgado, N. Cermak, V. C. Hecht, S. Son, Y. Li, S. M. Knudsen, S. Olcum, J. M. Higgins, J. Chen, W. H. Grover and S. R. Manalis, *PLoS One*, 2013, **8**, e67590.
24 M. Godin, F. F. Delgado, S. M. Son, W. H. Grover, A. K. Bryan, A. Tzur, P. Jorgensen, K. Payer, A. D. Grossman, M. W. Kirschner and S. R. Manalis, *Nat. Methods*, 2010, **7**, 387–390.
25 B. G. Nordestgaard and J. Rostgaard, *J. Microsc.*, 1985, **137**, 189–207.
26 K. Hotary, X. Y. Li, E. Allen, S. L. Stevens and S. J. Weiss, *Genes Dev.*, 2007, **21**, 1139–1139.
27 F. R. Turner and A. P. Mahowald, *Dev. Biol.*, 1979, **68**, 96–109.
28 F. R. Turner and A. P. Mahowald, *Dev. Biol.*, 1976, **50**, 95–108.
29 R. S. Richards, L. X. Wang and H. Jelinek, *Arch. Med. Res.*, 2007, **38**, 94–98.
30 L. C. S. Medeiros, W. De Souza, C. G. Jiao, H. Barrabin and K. Miranda, *PLoS One*, 2012, **7**, e33445.
31 O. Ohtani, *Arch. Histol. Cytol.*, 1987, **50**, 557–566.
32 M. Y. Fan, Z. P. Lum, X. W. Fu, L. Levesque, I. T. Tai and A. M. Sun, *Diabetes*, 1990, **39**, 519–522.
33 E. Sunami, H. Kanazawa, H. Hashizume, M. Takeda, K. Hatakeyama and T. Ushiki, *Arch. Histol. Cytol.*, 2001, **64**, 191–201.
34 V. Chandra, G. Swetha, S. Muthyala, A. K. Jaiswal, J. R. Bellare, P. D. Nair and R. R. Bhonde, *PLoS One*, 2011, **6**, e20615.
35 D. Terada, S. Hattori, T. Honda, M. Iitake and H. Kobayashi, *Microsc. Res. Tech.*, 2013, **76**, 290–295.

36 C. A. Morgan, N. Herman, P. A. White and G. Vesey, *J. Microbiol. Methods*, 2006, **66**, 183–193.
37 J. Malm, D. Giannaras, M. O. Riehle, N. Gadegaard and P. Sjovall, *Anal. Chem.*, 2009, **81**, 7197–7205.
38 B. D. Chan, F. Mateen, C. L. Chang, K. Icoz and C. A. Savran, *J. Microelectromech. Syst.*, 2012, **21**, 7–9.
39 B. D. Chan, K. Icoz, R. L. Gieseck and C. A. Savran, *IEEE Sens. J.*, 2013, **13**, 2857–2862.
40 G. G. Yaralioglu, A. Atalar, S. R. Manalis and C. F. Quate, *J. Appl. Phys.*, 1998, **83**, 7405–7415.
41 J. F. Shackelford and W. Alexander, *CRC materials science and engineering handbook*, CRC Press, Boca Raton, FL, 2001.
42 S. D. Senturia, *Microsystem design*, Kluwer Academic Publishers, Boston, 2001.
43 N. Lobontiu, I. Lupea, R. Ilic and H. G. Craighead, *J. Appl. Phys.*, 2008, **103**, 064306.
44 D. Hopwood, *Histochem. J.*, 1972, **4**, 267–303.
45 J. D. Bancroft and M. Gamble, *Theory and practice of histological techniques*, Churchill Livingstone, Edinburgh, 2008.
46 K. U. Laiho, J. D. Shelburn and B. F. Trump, *Am. J. Pathol.*, 1971, **65**, 203–214.
47 D. F. Bray, J. Bagu and P. Koegler, *Microsc. Res. Tech.*, 1993, **26**, 489–495.
48 J. C. Araujo, F. C. Teran, R. A. Oliveira, E. A. Nour, M. A. Montenegro, J. R. Campos and R. F. Vazoller, *J. Electron Microsc.*, 2003, **52**, 429–433.
49 J. T. Lee and K. L. Chow, *Scanning*, 2012, **34**, 12–25.
50 F. Braet, R. De Zanger and E. Wisse, *J. Microsc.*, 1997, **186**, 84–87.
51 J. L. Nation, *Stain Technol.*, 1983, **58**, 347–351.
52 N. H. Hazrin-Chong and M. Manefield, *J. Microbiol. Methods*, 2012, **90**, 96–99.
53 S. W. Jung, H. M. Joo, J. S. Park and J. H. Lee, *J. Appl. Phycol.*, 2010, **22**, 313–317.
54 N. Lobontiu, *Dynamics of microelectromechanical systems*, Springer, New York, 2007.
55 B. G. Durie and S. E. Salmon, *Cancer*, 1975, **36**, 842–854.
56 Z. N. Demidenko and M. V. Blagosklonny, *Aging*, 2009, **1**, 1008–1016.
57 K. Park, L. J. Millet, N. Kim, H. A. Li, X. Z. Jin, G. Popescu, N. R. Aluru, K. J. Hsia and R. Bashir, *Proc. Natl. Acad. Sci. U. S. A.*, 2010, **107**, 20691–20696.
58 T. T. Hansel, J. D. Pound, D. Pilling, G. D. Kitas, M. Salmon, T. A. Gentle, S. S. Lee and R. A. Thompson, *J. Immunol. Methods*, 1989, **122**, 97–103.
59 H. Bordelon, P. K. Russ, D. W. Wright and F. R. Haselton, *PLoS One*, 2013, **8**, e68369.
60 K. Hoshino, Y. Y. Huang, N. Lane, M. Huebschman, J. W. Uhr, E. P. Frenkel and X. J. Zhang, *Lab Chip*, 2011, **11**, 3449–3457.
61 C. L. Chang, C. A. Savran, S. Jalal and D. E. Matei, *IEEE Sens. J.*, 2012, 1672–1675.
62 K. Icoz and C. Savran, *Appl. Phys. Lett.*, 2010, **97**, 123701.
63 M. Marko, C. Hsieh, W. Moberlychan, C. A. Mannella and J. Frank, *J. Microsc.*, 2006, **222**, 42–47.

